Journal of Medicinal Chemistry

pubs.acs.org/jmc

Article

# Modulatory Role of Pantropic Cell Signaling Pathways in the Antimigratory and Antiproliferative Action of Triazole Chelated Iridium(III) Complexes in Cervical Cancer Cells

Anushka Mondal,[§] Bishnu Das,[§] Souvik Karmakar, Soumili Pani, Shrabani Khan, Parna Gupta,* and Jayasri Das Sarma*

Cite This: *J. Med. Chem.* 2024, 67, 20559−20570

Read Online

ACCESS | Metrics & More | Article Recommendations | Supporting Information

**ABSTRACT:** In the current study, the antimigratory and antiproliferative effect of three substituted triazole-chelated iridium(III) complexes Ir-TRN, Ir-TRH, and Ir-TRF were studied with special emphasis on modulation of P53 activity, a cell cycle regulator. ERK2/MAPK, another crucial cell signaling pathway protein, was also shown to play a crucial role in cell migration and proliferation. The complexes increase the ROS generation within the cell, further supporting apoptotic induction by exerting cellular oxidative stress. These metal complexes also affect ER stress by altering ERp29, an ER-resident chaperone, further inducing the process of apoptosis. The iridium(III) complexes restrict cervical cancer cell migration and proliferation by exerting pronounced effects as P53 activators and downregulation of ERK2/MAPK activity in cervical cancer cells. The underpinning mechanism of P53 and ERK2/MAPK activity in cervical cancer cells in the presence of iridium(III) complexes was studied in detail in this study, which paves the way for developing promising avenues for cancer therapeutics.

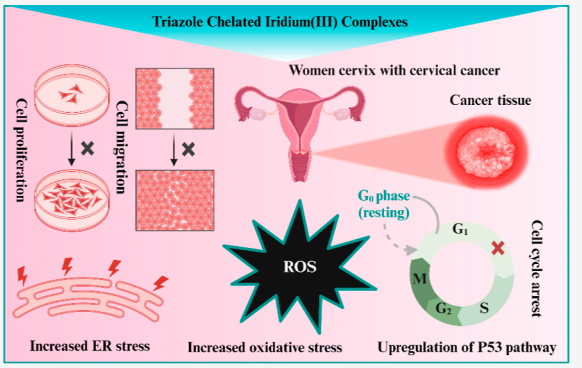


## INTRODUCTION

Cervical cancer ranks as the fourth most prevalent cancer among women worldwide.[1] The mortality rate of Cervical cancer is exceptionally high in areas lacking access to screening programs, preventive measures, and healthcare resources. Due to lack of treatment, advanced cervical cancer can metastasize to distant organs such as the lungs, liver, and bones, further reducing the survival rates.[2] Despite advancements in cancer treatment, cancer remains a major global health challenge, claiming millions of lives annually.[3] There is an urgent need for more effective and targeted therapies. Extensive research into effective cancer therapies has focused on novel molecular agents that modulate critical cellular pathways.[4]

The discovery of cisplatin in the 1960s marked the advent of metal-based cancer therapy, revolutionizing treatment with the subsequent development of platinum-based drugs like carboplatin and oxaliplatin.[5] However, challenges such as resistance and severe side effects have driven the search for alternative metal-based therapeutics.[6] This field has expanded to include other metal complexes such as ruthenium, gold, and iridium, each with unique mechanisms of action.[7] Metal-based cancer therapeutics continue to be explored and refined, offering promising treatment options.[8,9] Iridium(III) complexes, unlike platinum drugs, do not function as DNA alkylators but exhibit unique biological activities, including the generation of reactive oxygen species (ROS) and interactions with proteins and enzymes.[10,11] Their substitutional inertness enhances stability in biological environments, allowing for prolonged interactions with biomolecules, contributing to their anticancer effects.

The current study investigated the potential of three iridium(III) complexes Ir-TRN, Ir-TRH, and Ir-TRF each featuring a triazole moiety with varying attachments as therapeutics and emphasized the underlying cellular mechanism for cytotoxic behavior. We synthesized these complexes through a multistep process, starting with a copper-catalyzed azide−alkyne cycloaddition (CuAAC), followed by complexation with $[Ir(ppy)_2Cl]_2$ (ppy = 2-phenylpyridine). Our main objective was to evaluate the potential of these iridium(III) complexes to modulate specific cell signaling pathways that aid in regulating cell migration, Proliferation, and other metastatic properties.

Bi et al. and Jin et al. have reported on 2-phenylpyridine cyclometalated iridium(III) complexes designed primarily for

Received: August 25, 2024
Revised: October 29, 2024
Accepted: November 1, 2024
Published: November 11, 2024

**Scheme 1. Stepwise Synthesis of Triazole Ligands TRN, TRH, and TRF, and Their Corresponding Iridium(III) Complexes Ir-TRN, Ir-TRH, and Ir-TRF**

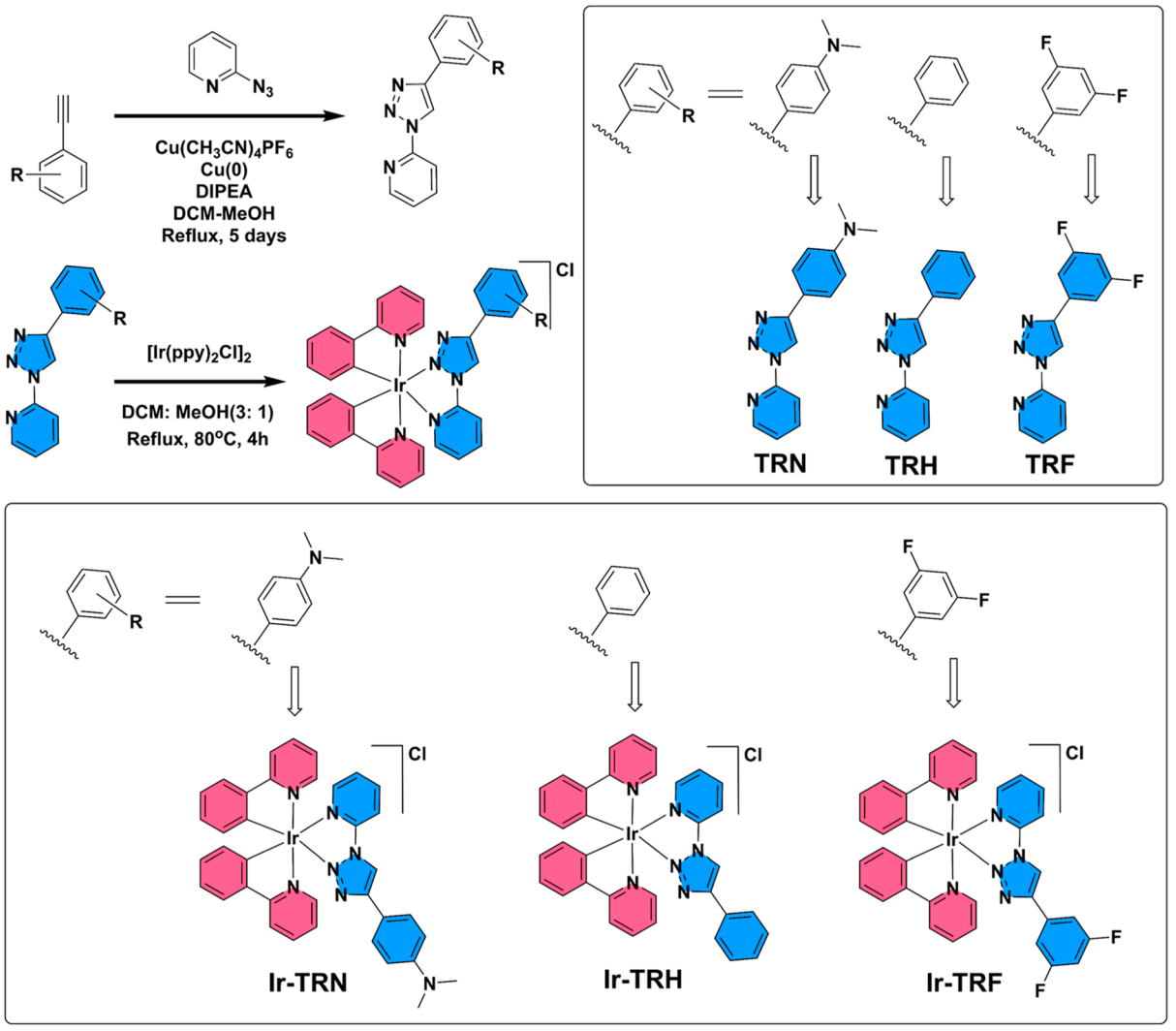


bioimaging applications, demonstrating low toxicity and high phototoxicity under light activation, making them effective agents for photodynamic therapy (PDT).[12,13] However, in contrast to these luminescent complexes, our research focuses on developing iridium(III) complexes specifically for therapeutic purposes, emphasizing selective cancer cell targeting and killing. By incorporating triazole systems as ancillary ligands with both electron-withdrawing and donating groups, we aim to enhance interactions with biological targets and increase cytotoxicity in cancer cells. Moreover, while conventional pyridyl triazoles are often favored for coordination to metal ions due to their structural properties,[14−17] Our study uniquely explores pyridyl 'inverse' triazoles. Although these inverse triazoles may exhibit lower coordination efficiency,[18] their unique electronic properties may confer distinct biological effects when coordinated to iridium(III) ions. Our investigation will provide insights into how these differences in coordination influence the biological activity and anticancer potential of the resulting complexes.

In vitro, treatment of the three iridium(III) complexes Ir-TRN, Ir-TRH, and Ir-TRF in metastatic cervical cancer cells ME180 demonstrated that these complexes upregulate P53 activity.[19] P53 is a crucial tumor suppressor gene that prevents cancer by monitoring DNA integrity and responding to cellular stresses like DNA damage and oncogene activation.[20,21] P53 also significantly induces cell cycle arrest at the G1/S checkpoint to ensure DNA integrity before synthesis. In many cancers, P53 can be inactivated, but restoring its function can help maintain genomic integrity, arrest the cell cycle, and prevent resistance to apoptosis.[22]

Treatment with these complexes also results in the downregulation of ERK2/MAPK activity in cervical cancer cells ME-180, thereby restricting migration and cell proliferation. ERK2/MAPK activates some of the transcription factors that induce the expression of genes involved in migration, like matrix metalloproteinases (MMPs).[23] ERK2/MAPK is also critical for regulating cell cycle progression, especially for transitioning from the G1 phase to the S phase, by activating cell cycle regulators such as cyclin D1.[24] Besides, when treated with these complexes, the cells generate reactive oxygen species (ROS), increasing oxidative stress in cancer cells through several critical mechanisms. Excess ROS induces significant DNA damage, including base modifications and strand breaks, overwhelming the cell's repair mechanisms and triggering apoptosis or necrosis.[25]


https://doi.org/10.1021/acs.jmedchem.4c01997
J. Med. Chem. 2024, 67, 20559−20570

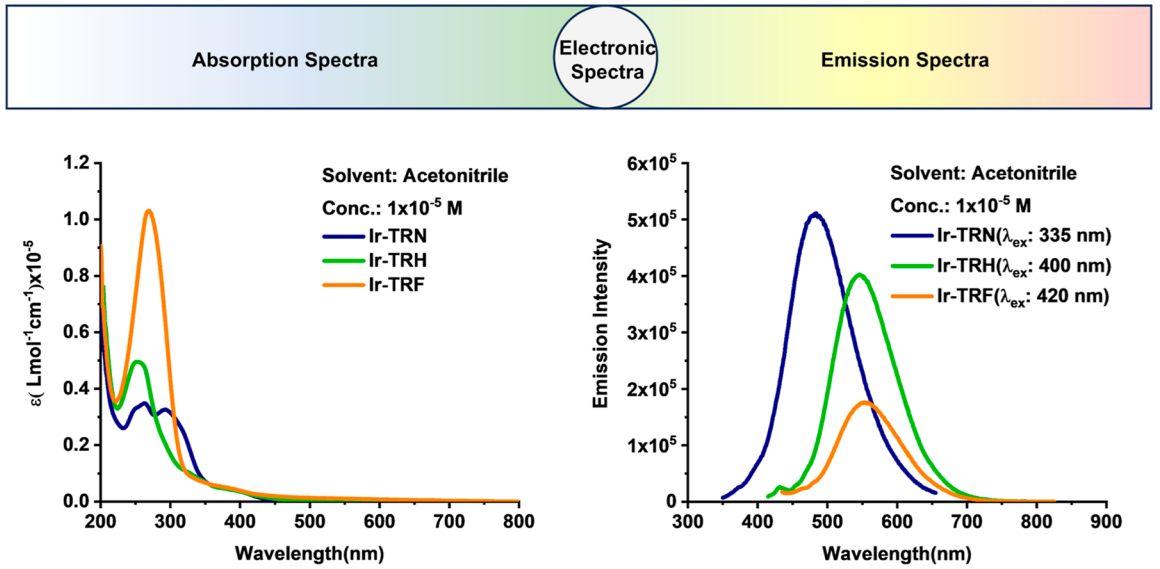


**Figure 1.** Absorption and emission spectra of Ir-TRN, Ir-TRH, and Ir-TRF in an acetonitrile solution.

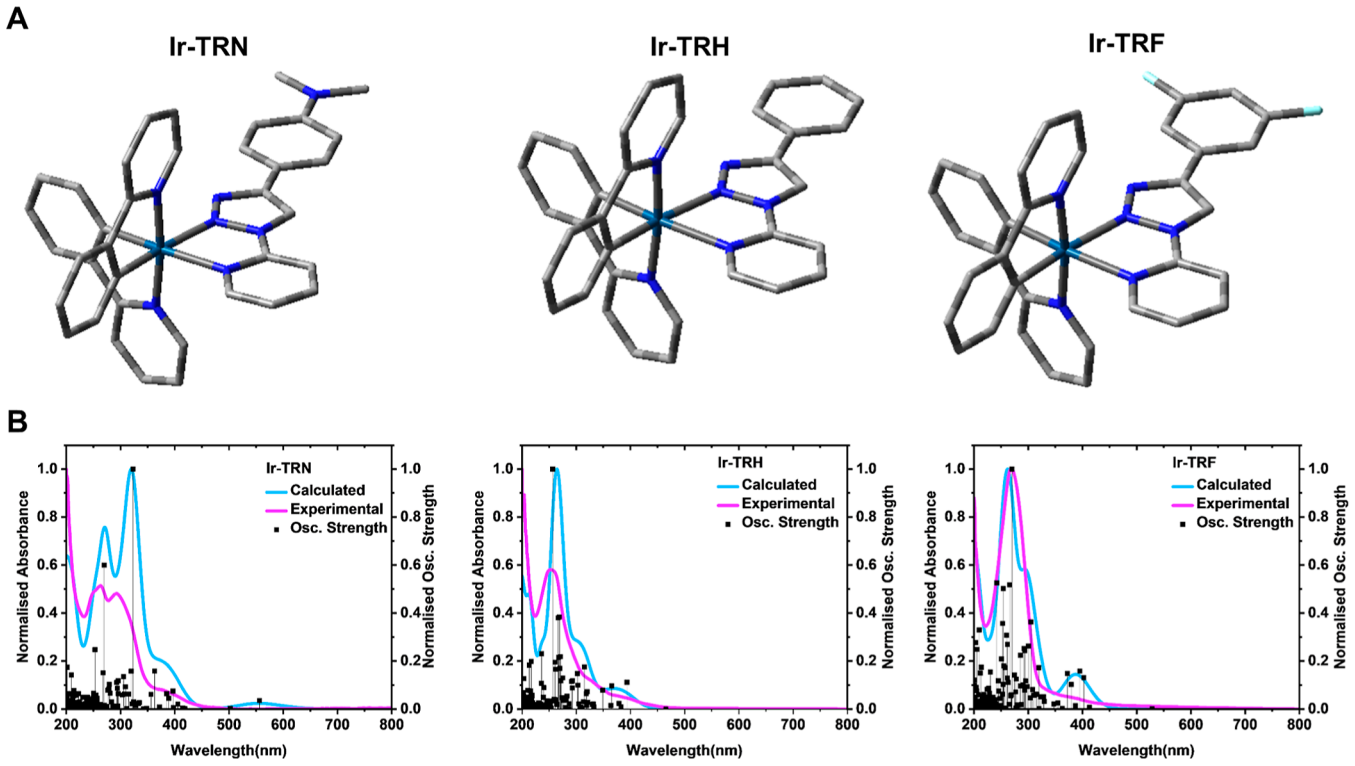


**Figure 2.** (a) Structures of Ir-TRN, Ir-TRH, and Ir-TRF as determined by DFT calculations, with hydrogen atoms omitted for clarity. The structures were visualized using GaussView. (b) Comparison of the calculated and experimentally obtained absorption spectra for Ir-TRN, Ir-TRH, and Ir-TRF, including the oscillator strengths for the transitions.

Moreover, treating these triazole-chelated iridium(III) complexes triggers the endoplasmic reticulum (ER) stress pathway, essential in maintaining cellular stress responses. Activation of the ER stress pathway disrupts normal cellular functions, accumulating misfolded proteins and subsequent stress responses.[26] Heightened stress response can drive cervical cancer cells more toward apoptosis. Our results suggest these iridium(III) complexes could be promising targets for developing new cancer therapeutics, providing valuable insights into their mechanisms of action and opening new avenues for more effective cancer treatments.

## RESULT AND DISCUSSION

**Synthesis.** The reaction of 2-azidopyridine with substituted phenylacetylene produces triazole ligands TRN, TRH, and TRF via azide−alkyne "click" reactions, following a reported procedure that utilizes $Cu(CH_3CN)_4PF_6$/Cu/DIPEA in a dichloromethane-methanol mixture under reflux for 5 days. The iridium(III) complexes Ir-TRN, Ir-TRH, and Ir-TRF were synthesized following a slightly modified procedure from the Watts Group.[27] A faint-yellow solution is obtained when $[Ir(ppy)_2Cl]_2$ is refluxed with TRH, TRN, and TRF,


https://doi.org/10.1021/acs.jmedchem.4c01997
J. Med. Chem. 2024, 67, 20559−20570

respectively, at 80 °C for 4 h in a 3:1 DCM-MeOH mixture and then dried to yield a yellow solid. This yellow solid was purified using thin layer chromatography with DCM/MeOH results in Ir-TRN, Ir-TRH, and Ir-TRF, as shown in Scheme 1. The CHN analysis data for Ir-TRN (C: 58.04, H: 4.04, N: 12.84), Ir-TRH (C: 55.46, H: 3.47, N: 11.11), and Ir-TRF (C: 55.44, H: 3.13, N: 11.10) confirm the empirical formulas: Ir-TRN: $C_{37}H_{31}IrN_7$, Ir-TRH: $C_{35}H_{26}ClIrN_6$, and Ir-TRF: $C_{35}H_{24}F_2IrN_6$. Furthermore, ESI-MS verifies the molecular composition of Ir-TRN, Ir-TRH, and Ir-TRF as $[Ir(ppy)_2(TRN)]Cl$ $[Ir(ppy)_2(TRH)]Cl$, and $[Ir(ppy)_2(TRF)]Cl$, respectively. The observed mass patterns align with the simulated ones, supporting the accuracy of the findings (Figures S1−S3). Additionally, the identity and purity of the complexes were confirmed through $^1H$, $^{13}C$, and $^{19}F$ NMR spectra, as well as HPLC (Figures S4−S14). Singlet state geometries were optimized using the density functional hybrid model B3LYP with the 6−31g(d,p) basis set for C, H, N, and O and the Def2TZVP basis set for Ir.[28] The geometry-optimized structures of Ir-TRN, Ir-TRH, and Ir-TRF reveal the arrangement of the metal center (Figure 2).

**Electronic Spectroscopy.** The absorption and emission spectra of the Ir-TRN, Ir-TRH, and Ir-TRF complexes in acetonitrile are depicted in Figure 1. The experimental absorption ($\lambda_{abs}$) and emission ($\lambda_{em}$) maxima for each complex are summarized in Table 1. The absorption spectra of the three

**Table 1. Experimental Absorption ($\lambda_{abs}$) and Emission ($\lambda_{em}$) of Ir-TRN, Ir-TRH, and Ir-TRF Were Obtained from Their Respective Graphs**

| complexes | $\lambda_{abs}$ [nm] | $\lambda_{em}$ [nm] |
|---|---|---|
| Ir-TRN | 247.9(0.3247), 263.8(0.3483), 293.45(0.3262), 320.65(0.2345), 378.2(0.0501), 405.15(0.0325), 472.05(0.0009) | 484 |
| Ir-TRH | 254.65(0.4948), 294.95(0.1927), 327.65(0.1013), 353.2(0.0648), 383.4(0.0440), 400.25(0.0354) | 546 |
| Ir-TRF | 269.9(1.0304), 347.55(0.0692), 382.4(0.0483), 452.9(0.0188) | 557 |

complexes exhibit multiple absorption bands within the UV−visible region, indicating their photophysical activity. Ir-TRN and Ir-TRH exhibit similar absorption features, indicating comparable electronic environments, with both ligand-centered ($\pi \rightarrow \pi^*$) and metal-to-ligand charge transfer (MLCT) transitions. In contrast, Ir-TRF shows a red-shift in its absorption maximum at 452.90 nm, suggesting stronger metal−ligand interactions and enhanced MLCT character. This shift indicates that Ir-TRF has a more pronounced metal−ligand bonding compared to the other two complexes. Ir-TRN exhibits emission at 484 nm, which is blue-shifted compared to Ir-TRH, indicating a higher energy emission. This shift may be attributed to a less extended conjugation in the ligand structure, leading to a less stabilized excited state. In contrast, Ir-TRH emits at 546 nm, a wavelength typical of metal-to-ligand charge transfer (MLCT) emission in iridium-(III) complexes, reflecting the balanced interaction between the metal center and the ligand. Ir-TRF shows the most red-shifted emission at 557 nm, suggesting that its ligand framework stabilizes the excited state more effectively, resulting in lower energy emission. This red-shift in emission also correlates with the higher wavelength absorption band observed at 452.90 nm, indicating stronger metal−ligand interactions in Ir-TRF.

Theoretical calculations provide detailed insights into the electronic transitions of the complexes (Figures S15−S17; Tables S1−S3). For Ir-TRN, a primary LC transition is identified at 556.2324 nm, involving a transition from HOMO to LUMO with a 99% contribution from triazole-*N*,*N*-dimethylaniline to triazole-pyridine. At 502.5911 nm, the transition involves HOMO−1 to LUMO with a 98% contribution from Ir-ppy to triazole-pyridine, indicating an MLCT transition. Other significant transitions at 396.8383, 385.1637, and 362.6966 nm involve contributions from Ir-ppy to triazole-pyridine and other ppy-related transitions, representing MLCT and LC transitions. For Ir-TRH, a significant metal-to-ligand charge transfer (MLCT) transition occurs at 465.5459 nm, predominantly involving a transition from the highest occupied molecular orbital (HOMO) to the lowest unoccupied molecular orbital (LUMO) with a 98% contribution from Ir-ppy to pyridine-triazole. Another notable transition at 393.7506 nm, involves a HOMO to LUMO+1 transition with a 95% contribution from Ir-ppy to ppy, indicating a ligand-centered (MLCT) transition. Additional transitions are observed at 365.7243 nm, involving multiple orbital contributions, and at 349.1529 nm, primarily from HOMO−3 to LUMO and HOMO−2 to LUMO, with significant contributions from Ir-ppy-triazole-phenyl and triazole-pyridine, indicating both MLCT and LC characteristics. For Ir-TRF, a significant MLCT transition occurs at 528.3567 nm with an oscillator strength of 0.0004, involving a transition from HOMO to LUMO with a 98% contribution from Ir-Phenyl of ppy to triazole-pyridine. At 395.1939 nm, the transition involves multiple orbital contributions, including HOMO to LUMO+1 and HOMO to LUMO+2, with significant contributions from Ir-phenyl of ppy to ppy-pyridine and triazole-pyridine-1,3-difluorophenyl, indicating MLCT transitions. Additional transitions at 372.3025, 305.1693, and 285.8952 nm involve combinations of Ir-Phenyl of ppy and various triazole-pyridine transitions, showing a mixture of MLCT and LC characteristics.

The comparison between the calculated and experimentally obtained absorption spectra for Ir-TRN, Ir-TRH, and Ir-TRF shows a good correlation, validating the theoretical models used. The calculated spectra include the oscillator strengths for the transitions, providing insights into the nature and intensity of the electronic transitions.

**Cytotoxic Effects of Iridium(III) Complexes.** The cytotoxicity of three different iridium(III) complexes Ir-TRN, Ir-TRH, and Ir-TRF was evaluated through MTT(3-(4, 5-dimethyl thiazolyl-2)-2, 5-diphenyltetrazolium bromide) assays to measure their effects on cell viability. These assays were conducted on three cell lines, including ME-180 cervical cancer cells (Figure 3A), A549 lung carcinoma cells (Figure 3B), and human keratinocytes (noncancerous, Figure 3C). In ME-180 cells, all three complexes showed potent cytotoxic effects, with $IC_{50}$ values of 14.48 $\mu$M for Ir-TRN, 14.02 $\mu$M for Ir-TRH, and 11.45 $\mu$M for Ir-TRF. Among these, Ir-TRF exhibited the highest potency, as reflected by its lowest $IC_{50}$ value. As the concentration of these iridium(III) complexes increased, cell viability significantly decreased, leading to near-complete cell death at the highest concentrations tested. These findings suggest strong potential for these compounds as anticancer agents, particularly in targeting cervical cancer cells. For A549 lung carcinoma cells, the complexes exhibited reduced cytotoxicity compared to ME-180, with higher $IC_{50}$ values of 29.51 $\mu$M for Ir-TRN, 32.47 $\mu$M for Ir-TRH, and


https://doi.org/10.1021/acs.jmedchem.4c01997
J. Med. Chem. 2024, 67, 20559−20570

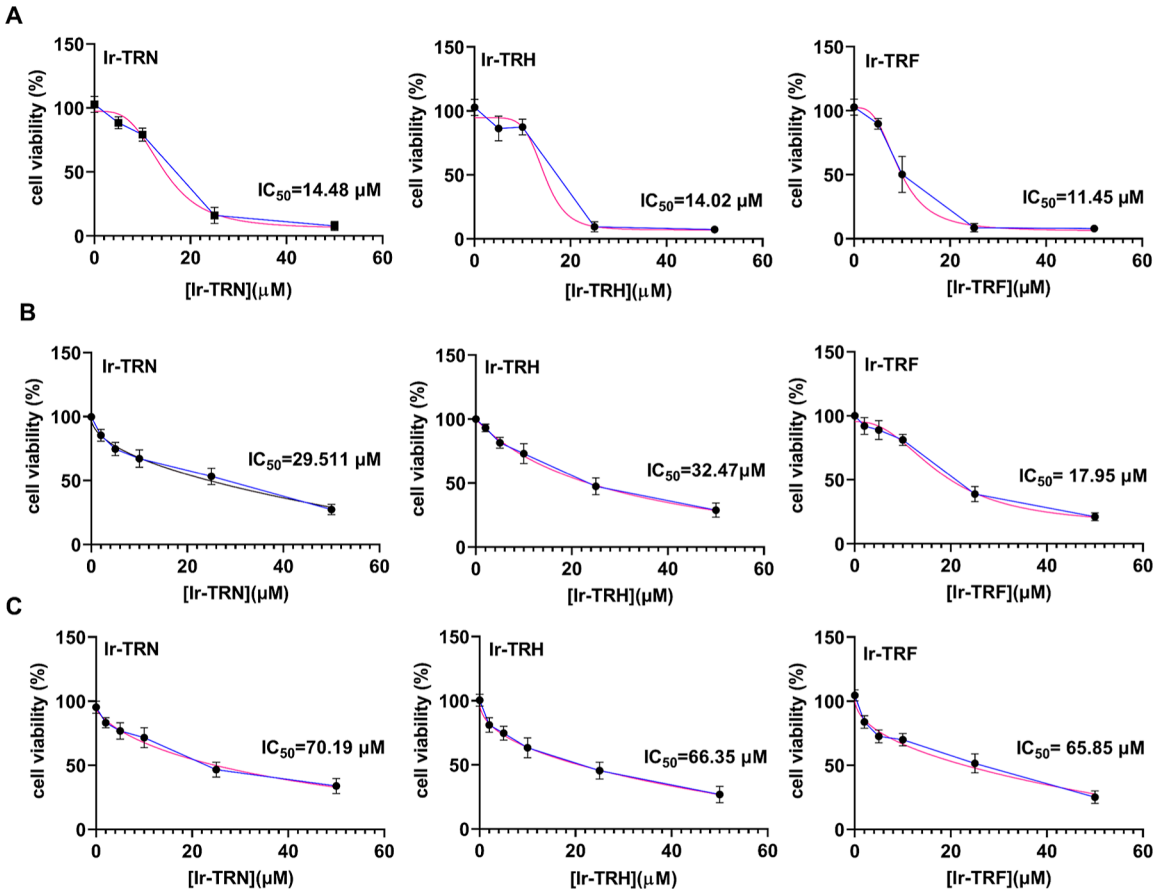


**Figure 3.** Cytotoxic effects of iridium(III) complexes on ME-180, A549, and human keratinocyte cells. Cell viability was assessed using the MTT assay with increasing concentrations (0−60 $\mu$M) of Ir-TRN, Ir-TRH, and Ir-TRF. (A) ME-180 cervical cancer cells showed potent cytotoxic effects, with Ir-TRF exhibiting the greatest potency. (B) A549 lung carcinoma cells demonstrated moderate sensitivity to all complexes. (C) Human keratinocytes HaCaT (noncancerous cells) displayed the lowest cytotoxicity, indicating selective effects on cancer cells. Data represent mean ± SD from three experiments.

17.95 $\mu$M for Ir-TRF. Ir-TRF still showed the strongest cytotoxicity among the three complexes, though less potent than its effects on cervical cancer cells. In human keratinocytes, a noncancerous cell line, the cytotoxic effects were much weaker, with $IC_{50}$ values of 70.19 $\mu$M for Ir-TRN, 66.35 $\mu$M for Ir-TRH, and 65.85 $\mu$M for Ir-TRF. These higher $IC_{50}$ values indicate that the complexes are less toxic to noncancerous cells, supporting their selective cytotoxicity toward cancer cells. To confirm the MTT assay results, a Trypan Blue exclusion assay was performed (Figure S4). This assay measured live cell populations after treatment with the complexes at their respective $IC_{50}$ concentrations. Consistent with the MTT data, Ir-TRN, Ir-TRH, and Ir-TRF treatments led to approximately 50% cell viability, further confirming the significant cytotoxic effects observed.

**Inhibition of Cell Migration and Proliferation through Modulation of Signaling Pathways.** Next, we wanted to check cell migration and Proliferation as these properties mark the two most crucial phenomena observed in the Metastasis of cancer cells. Figure 4A and 4B show that all three complexes restricted cell migration. Confluent monolayers of cervical cancer cells were incubated with the test complexes for 24 h after creating a scratch/wound, termed a "scratch assay." The migration of cells toward the "wound area" was monitored by acquiring bright-field images at different time points. At 12 h, the percentage of wound closure was markedly reduced in cells treated with Ir-TRN, Ir-TRH, and Ir-TRF, with Ir-TRH showing the most significant inhibition. This inhibitory effect was more pronounced at 24 h, with Ir-TRH maintaining the highest level of migration inhibition. Western blot analysis (Figure 4C, D) revealed a significant decrease in Erk/MAPK protein expression in cells treated with the iridium(III) complexes concerning the control to the control, with Ir-TRN causing the most substantial reduction, followed by Ir-TRH and Ir-TRF. These results suggest that the downregulation of Erk/MAPK, a crucial signaling pathway controlling cell migration, Proliferation, and survival, could be a mechanism through which these complexes exert their effects.

Additionally, Figure 4E demonstrates that the test complexes can significantly affect cancer cell proliferation. A clonogenic assay was performed where 500−800 cells were seeded in 60 mm dishes. After 1 week of incubation, it was seen that all of the three complexes were able to restrict cancer cell proliferation. All three complexes were treated at an $IC_{25}$ dose for cell migration and proliferation assay. Ir-TRF restricts cell proliferation a little less than the other complexes. However, the number of colonies formed and the size of the colony formation are still restricted by Ir-TRF. Comparing the three complexes, Ir-TRH is the best for impairing cell migration, and Ir-TRN and Ir-TRH both work well for restricting cell proliferation. The combined data from the


https://doi.org/10.1021/acs.jmedchem.4c01997
J. Med. Chem. 2024, 67, 20559−20570

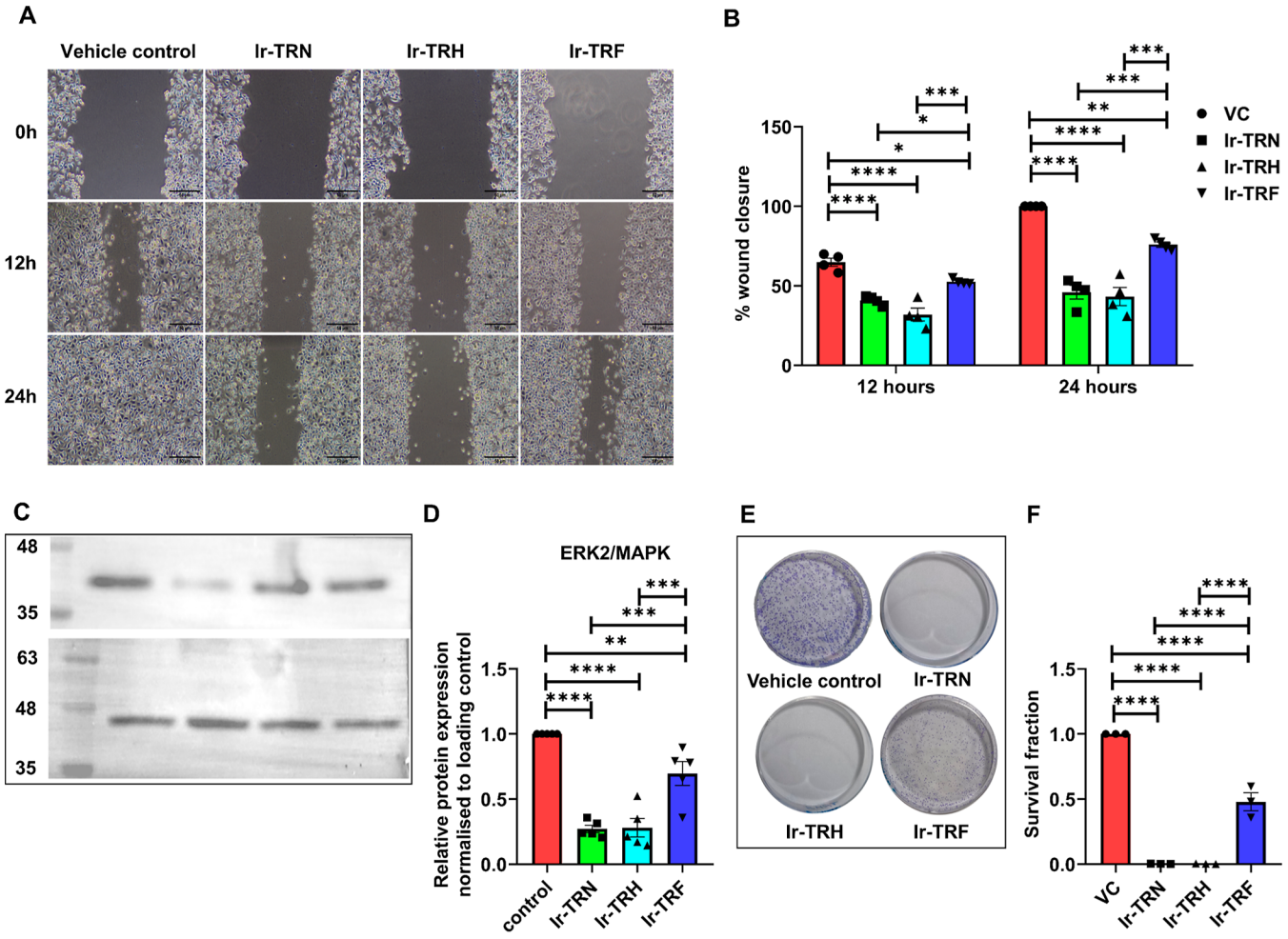


**Figure 4.** Iridium(III) complexes restrict Cell migration and Proliferation through modulation of the ERK2/MAPK pathway. (A and B): Wound healing assay shows significant inhibition of cervical cancer cell migration by Ir-TRN, Ir-TRH, and Ir-TRF compared to vehicle control (VC) at 12 and 24 h. (C and D): Western blot analysis reveals reduced Erk/MAPK protein expression in cervical cancer cells treated with Ir-TRN, Ir-TRH, and Ir-TRF compared to vehicle control. E and F: Clonogenic assay demonstrates a decreased survival fraction of cervical cancer cells treated with Ir-TRN, Ir-TRH, and Ir-TRF compared to untreated cells.

wound healing, Western blot, and clonogenic assays highlight the therapeutic potential of Ir-TRN, Ir-TRH, and Ir-TRF. These iridium(III) complexes reduce cell viability, impair cell migration, downregulate crucial signaling proteins, and inhibit long-term cell survival. Among them, Ir-TRN emerges as the most promising candidate for further development as a therapeutic agent for cervical cancer due to its superior efficacy in all assays performed.

**Inhibition of Cell Cycle Progression via Upregulation of P53 Expression.** Flow cytometry analysis, as shown in Figure 5A, B, demonstrates the cell cycle progression of samples treated with these complexes for 24 h of incubation, revealed that Ir-TRN and Ir-TRH treatment resulted in a marked increase in the restriction of cells in the G0/G1 phase, accompanied by a decrease in cells in the S and G2/M phases, compared to the vehicle control and other treatments. This indicates that Ir-TRN and Ir-TRH induce a G1/S phase arrest, inhibiting cell division. Western blot analysis (C and D) further demonstrated that Ir-TRN and Ir-TRH significantly upregulated P53 expression levels compared to the vehicle control and other treatments. The quantitative analysis showed a substantial increase in P53 protein level, normalized to $\gamma$-actin, following Ir-TRN and Ir-TRH treatment. Since P53 is a primary checkpoint regulator of cell cycle division at the G1/S phase, significant upregulation of P53 by these complexes suggests a mechanism of action of Ir-TRN and Ir-TRH involved in restricting cell division at the G1/S phase.

**ROS Production Induced Oxidative Stress in Cervical Cancer Cells.** Figure 6A presents flow cytometry histograms illustrating the fluorescence intensity of DCFDA, which indicates ROS levels in cells treated with control, Ir-TRN, Ir-TRH, and Ir-TRF. The overlay of histograms reveals a marked increase in fluorescence intensity in Ir-TRN and Ir-TRH treated cells compared to the control and Ir-TRF treated cells. The quantitative analysis in Figure 6B confirms these observations, showing a significant increase in mean fluorescence intensity in Ir-TRN and Ir-TRH treated cells relative to the control ($*p < 0.05$, $**p < 0.01$, $***p < 0.001$). These results suggest that Ir-TRN and Ir-TRH treatments elevate intracellular ROS levels more effectively than Ir-TRF and control treatments, thereby generating more oxidative stress in cervical cancer cells. Data suggest that reactive oxygen species (ROS) may act as mediators in generating cellular stress following these treatments.

**Iridium(III) Complexes Trigger ER-Stressed-Induced Apoptosis.** The iridium(III) complexes trigger ER stress-


https://doi.org/10.1021/acs.jmedchem.4c01997
J. Med. Chem. 2024, 67, 20559−20570

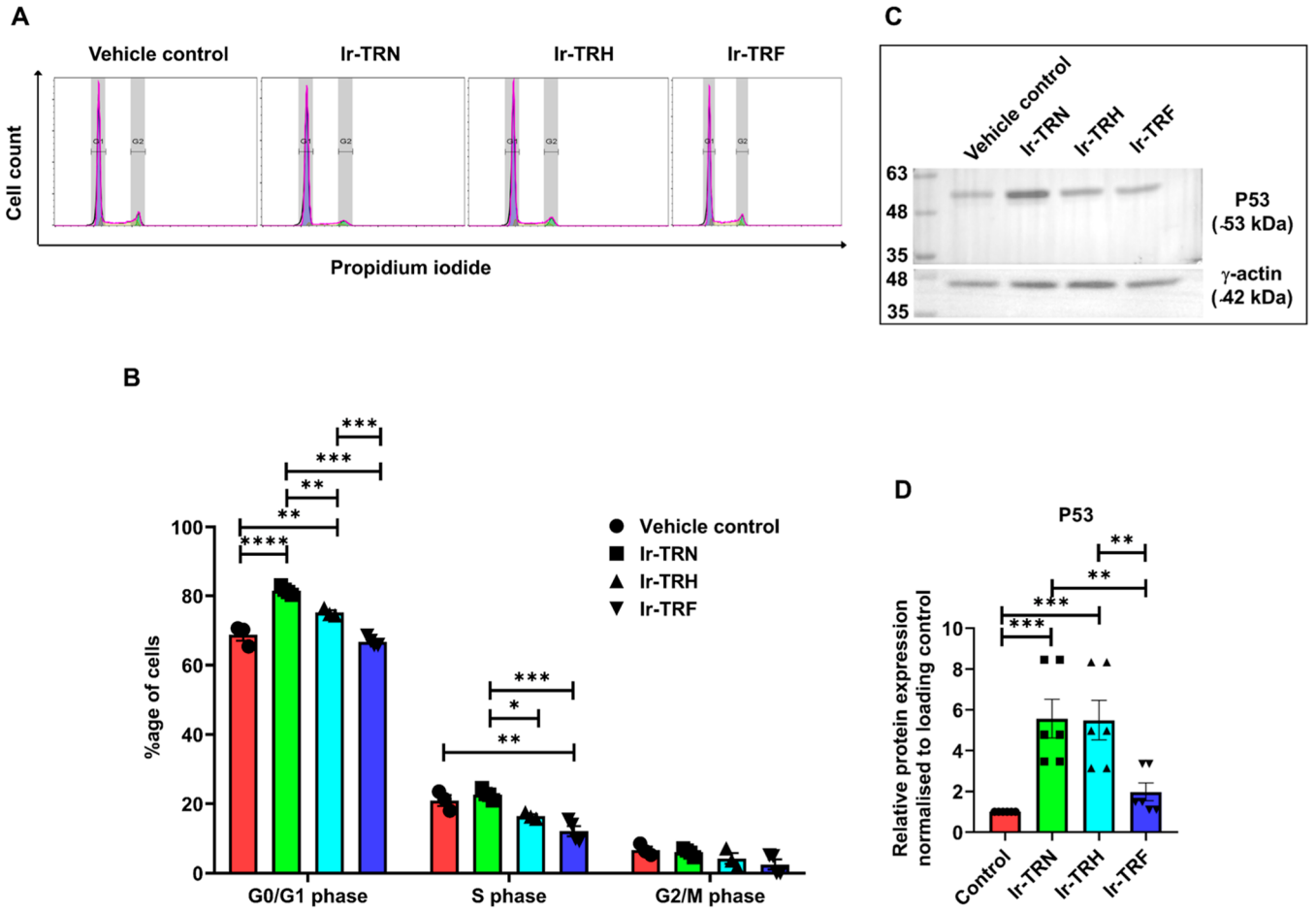


**Figure 5.** Ir-TRN and Ir-TRH significantly upregulated P53, restricting cell cycle division at the G1/S phase. (A) Flow cytometry histograms demonstrating cell cycle distribution after treatment with iridium(III) complexes. (B) Quantitative analysis of cell cycle phases showing a significant increase in G0/G1 phase with Ir-TRN and Ir-TRH (*$p < 0.05$, **$p < 0.01$, ***$p < 0.001$). (C) Following treatment with these complexes, Western blot analysis of P53 and $\gamma$-actin demonstrates significant upregulation of P53 in Ir-TRN and Ir-TRH. (D) Quantitative analysis of P53 levels normalized to $\gamma$-actin showing significant upregulation with Ir-TRN and Ir-TRH (*$p < 0.05$, **$p < 0.01$, ***$p < 0.001$).

induced apoptosis in cervical cancer cells, as demonstrated by Propidium Iodide staining in Figure 7A–D. ERp29 is an ER-resident chaperone protein that helps in the trafficking of proteins. Upregulation of ERp29 induces ER stress by accumulating unfolded or misfolded proteins, which then triggers the Unfolded Protein Response (UPR) pathway.[29] While this pathway aims to restore normal cellular function, severe and prolonged ER stress activates the apoptotic pathways. ERp29 also helps activate CHOP/GADD153, a transcription factor responsible for upregulating pro-apoptotic proteins and downregulating antiapoptotic proteins such as Bcl2, thereby causing apoptosis.[30] Additionally, ER stress can also enhance the activation of caspases, particularly caspase-3, which plays a crucial role in the execution phase of apoptosis.[31]

Western blot analyses reveal that treatments with Ir-TRN, Ir-TRH, and Ir-TRF led to differential expression of ERp29 compared to the control. The loading control, $\gamma$-Actin, confirms equal protein loading across the samples. So, Ir-TRN and Ir-TRH, in particular, elicit a robust stress response in cervical cancer cells, highlighting their potential as therapeutic agents in inducing stress-mediated apoptosis or growth inhibition in cancer treatment (*$p < 0.05$, **$p < 0.01$, ***$p < 0.001$).

## CONCLUSION

This current study demonstrated the efficacy of the three triazole-chelated iridium(III) complexes, Ir-TRN, Ir-TRH, and Ir-TRF, individually to restrict cell migration and Proliferation via cell cycle arrest. These iridium(III) complexes also induce apoptosis by increasing ER stress and oxidative stress pathways. Iridium(III) complexes are known for their anticancer properties through regulating the P53 pathway, a known tumor-suppressive gene. Our study also observed that P53 is activated after treatment with these novel complexes Ir-TRN, Ir-TRH, and Ir-TRF, further leading to cell cycle arrest at the G1/S phase. The novelty of our study lies in exploring the underpinning mechanism of restricting cell migration and cell proliferation via the downregulation of the ERK2/MAPK pathway. Upregulation of ERp29 further demonstrated the potency of the iridium(III) complexes in promoting apoptosis. Among the three complexes, Ir-TRF is the most cytotoxic for all cell lines, however, Ir-TRN stands out as the most effective compared to Ir-TRH and Ir-TRF given its comprehensive role in restricting cancer metastasis. Our research investigated the efficacy of iridium(III) complexes in inhibiting the acute characteristics of cancer cells that contribute to their metastatic potential.


https://doi.org/10.1021/acs.jmedchem.4c01997
J. Med. Chem. 2024, 67, 20559–20570

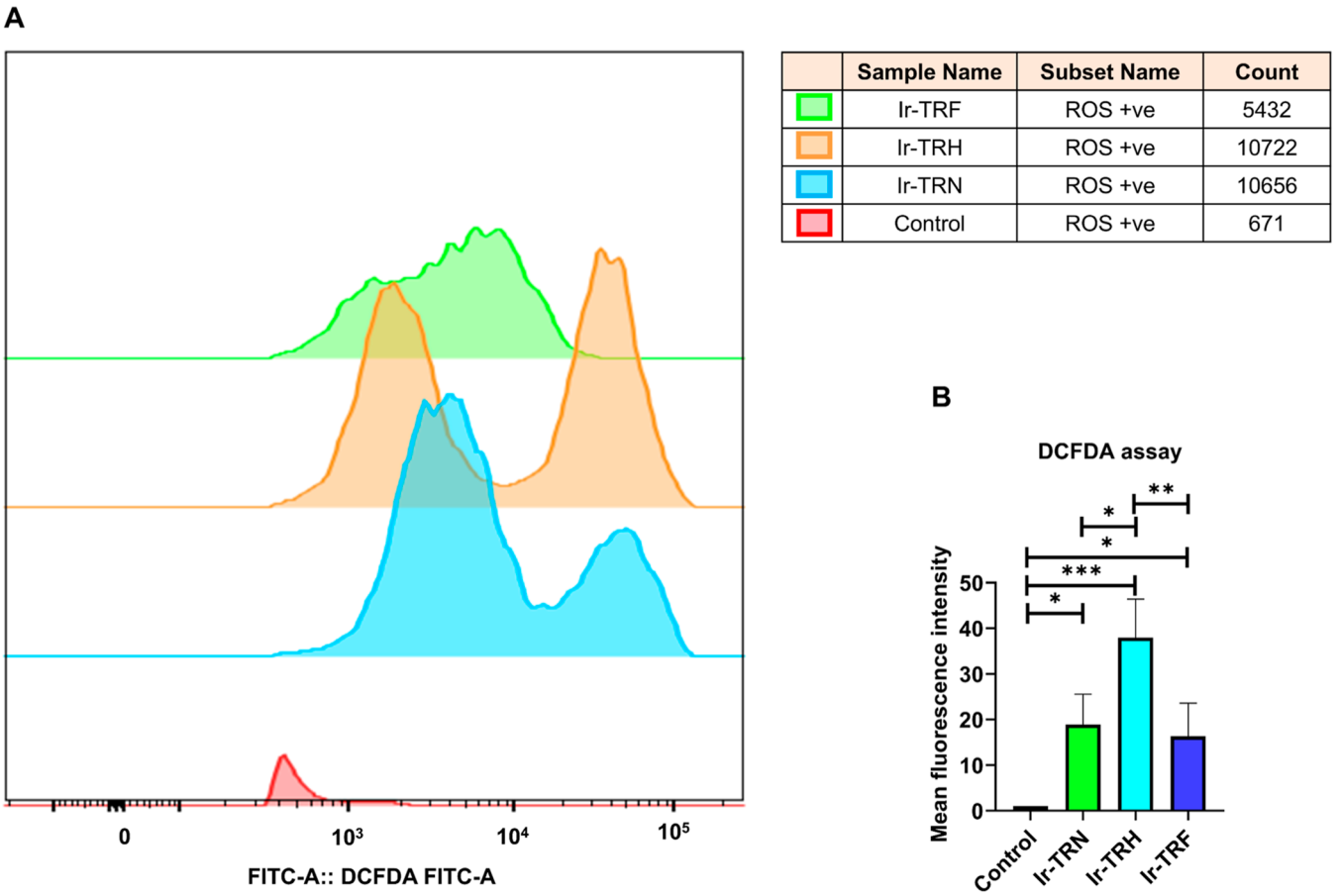


**Figure 6.** Measurement of ROS levels of complexes using the DCFDA assay. (A) Overlay of flow cytometry histograms displaying DCFDA fluorescence intensity for each complex. Fluorescence intensity, indicating ROS levels, was measured using FITC-A: DCFDA FITC-A. The complexes include Ir-TRF (green), Ir-TRH (orange), Ir-TRN (blue), and Control (red). The table on the right provides cell counts for complexes. (B) Quantitative analysis of mean fluorescence intensity indicates significantly higher ROS levels in Ir-TRN and Ir-TRH treated cells compared to control and Ir-TRF ($*p < 0.05$, $**p < 0.01$, $***p < 0.001$).

## MATERIALS AND METHODS

The starting materials, including $IrCl_3 \cdot 3H_2O$, 2-phenylpyridine, 2-bromopyridine, ethynylbenzene, 4-ethynyl-*N*,*N*-dimethylaniline, and 1-ethynyl-3,5-difluorobenzene, were sourced from Sigma-Aldrich and used as received without any further purification. Anhydrous methanol and acetonitrile were also obtained from Sigma-Aldrich. Other solvents of analytical grade were acquired from commercial suppliers and were dried using standard methods before use.

**Instrumental Methods.** Elemental analysis was performed using a PerkinElmer CHN Analyzer (2400 series). Mass spectra (ESI-MS) were obtained in positive mode electrospray ionization with a Bruker maXis IITM instrument. NMR spectra ($^1H$ and $^{13}C$) were recorded using JEOL ECS 400 and Bruker-500 spectrometers. Coupling constants (J) are given in hertz, and chemical shifts are reported in parts per million ($\delta$) relative to $CDCl_3$, which was used as an external reference (7.26 ppm for $^1H$ and 77.16 ppm for $^{13}C$).

**Optical Measurements.** Absorption spectra of the complex were measured with a Jasco V-670 spectrophotometer. Emission spectra at room temperature in solution were recorded using a Fluoro-max3 spectrofluorometer from Horiba Jobin Yvon.

**Computational Methodologies.** The optimization of structures, as well as the computation of UV−vis and emission spectra, was carried out using both ground state and time-dependent density functional theory (TD-DFT). All calculations were performed using Gaussian 16 software. Singlet state geometries were optimized, and the properties of excited states were calculated with the B3LYP density functional hybrid model, utilizing the 6-31G(d,p) basis set for C, H, N, O atoms, and the Def2TZVP basis set for Ir atoms. Theoretical electronic transitions were determined using GaussSum software. Additionally, Chemcraft 1.8 software was used to derive Frontier molecular orbitals from the generated fchk file.

**Synthetic Procedures.** *Synthesis of Ligands.* TRN: 2-azidopyridine (330.8 mg, 2.7547 mmol), and 4-ethynyl-*N*,*N*-dimethylaniline (400 mg, 2.7547 mmol) were dissolved in 28 mL $CH_2Cl_2$, and 7 mL methanol, and the solution was degassed. Cu $(CH_3CN)_4PF_6$ (205 mg, 0.55 mmol), Cu (34.9 mg, 0.55 mmol), and DIPEA (960 $\mu$L, 5.5094 mmol) was added, and it was added under reflux for 5 days. After cooling to room temperature, water and $CH_2Cl_2$ were added. After stirring the solution vigorously for some minutes, the layers were separated, and the aqueous layers were extracted with $CH_2Cl_2$ and dried over $Na_2SO_4$. The solvent was removed under vacuum and purified by column chromatography on silica gel and $CH_2Cl_2$-hexane as eluent. The product was obtained as a white solid. Yield: 392 mg (53%).

TRH: 2-azidopyridine (588 mg, 4.895 mmol), and ethynylbenzene (500 mg, 4.895 mmol) were dissolved in 64 mL $CH_2Cl_2$ and 16 mL methanol, and the solution was degassed. $Cu(CH_3CN)_4PF_6$ (364.6 mg, 0.978 mmol), Cu (62 mg, 0.978 mmol), and DIPEA (1700 $\mu$L, 9.79 mmol) were added and it was added under reflux for 5 days. After cooling to room temperature, water and $CH_2Cl_2$ were added. After stirring the solution vigorously for some minutes, the layers were separated and the aqueous layers were extracted with $CH_2Cl_2$ dried over $Na_2SO_4$. The solvent was removed under vacuum and it was purified by column chromatography on silica gel and $CH_2Cl_2$-hexane as eluent. The product was obtained as a white solid. Yield: 472 mg (43%).


https://doi.org/10.1021/acs.jmedchem.4c01997
J. Med. Chem. 2024, 67, 20559−20570

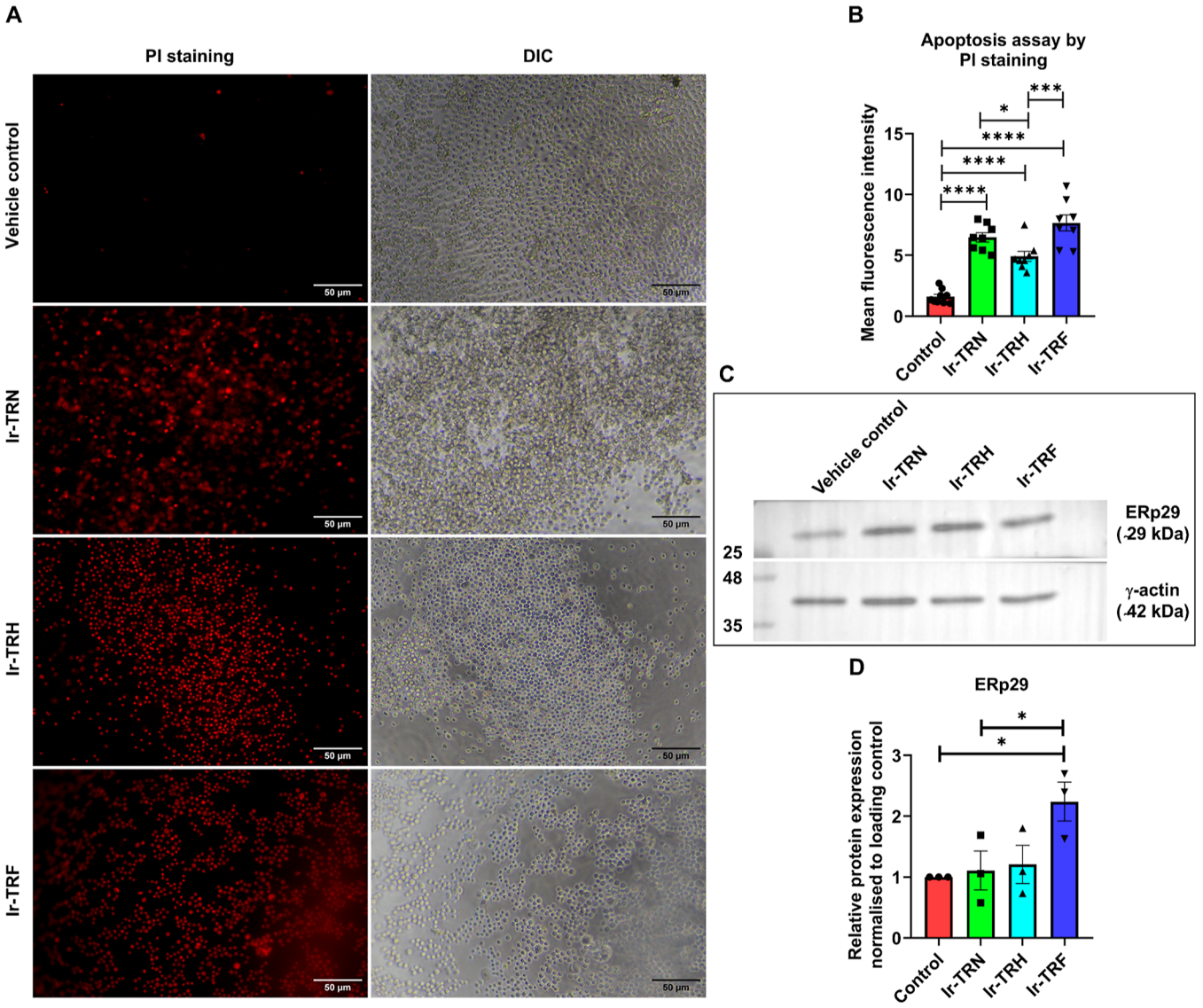


**Figure 7.** Iridium(III) complexes trigger ER stress-induced apoptosis in cervical cancer cells (A) DIC and IX81 fluorescence images of live ME-180 cells stained with PI were obtained after treating the cells with iridium(III) complexes to get a count of PI-positive cells compared to control cells. (C) Western blot of ERp29 and $\gamma$-actin after treatment with iridium(III) complexes demonstrates significant upregulation of ERp29 in Ir-TRF compared to control. (D) Quantitative analysis of ERp29 levels normalized to $\gamma$-actin showing significant upregulation with Ir-TRN and Ir-TRH(*$p$ < 0.05, **$p$ < 0.01, ***$p$ < 0.001).

TRF: 2-azidopyridine (391.3 mg, 3.2581 mmol), and 1-ethynyl-3,5-difluorobenzene (450 mg, 3.2581 mmol) were dissolved in 36 mL $CH_2Cl_2$ and 9 mL methanol, and the solution was degassed. $Cu(CH_3CN)_4PF_6$ (242.2 mg, 0.65 mmol), Cu (41.2 mg, 0.65 mmol), and DIPEA (1135 $\mu$L, 6.5162 mmol) were added and it was added under reflux for 5 days. After cooling to room temperature, water and $CH_2Cl_2$ were added. After stirring the solution vigorously for some minutes, the layers were separated, and the aqueous layers were extracted with $CH_2Cl_2$ and dried over $Na_2SO_4$. The solvent was removed under vacuum and it was purified by column chromatography on silica gel and $CH_2Cl_2$-hexane as eluent. The product was obtained as a white solid. Yield: 434 mg (51%).

**Synthesis of Complexes.** Ir-TRN: TRN (24.72 mg, 0.0932 mmol) was refluxed 4 h at 80 °C with $[Ir(ppy)_2]_2Cl_2$ (50 mg, 0.0932 mmol) in dichloromethane and methanol (3:1) solution to afford a reddish-orange colored solution. The solvent was evaporated under reduced pressure. The reddish-orange solid so obtained was redissolved in the minimum amount of dichloromethane and purified by a thin layer chromatography technique using 5% methanol in $CH_2Cl_2$. The desired orange solution was collected and dried under reduced pressure. Yield: 44 mg (61%). HPLC Purity: ≥ 97%. ESI-MS: Observed: $M^+$ = 766.2270; Exact: $M^+$ = 766.2267. $^1$H NMR (500 MHz, $CDCl_3$, $\delta$)(ppm): 10.92(1H, s), 9.73(1H, d, $J$ = 8.10), 8.37(1H, t, $J$ = 7.75), 7.90(2H, t, $J$ = 8.50), 7.85(2H, d, $J$ = 8.85), 7.76(2H, t, $J$ = 7.80), 7.72(2H, t, $J$ = 6.40), 7.66(2H, d, $J$ = 6.55), 7.51(1H, d, $J$ = 5.80), 7.34(1H, t, $J$ = 7.50), 7.05−6.97(4H, m), 6.92−6.87(2H, m), 6.66(2H, d, $J$ = 9.00), 6.28(2H, d, $J$ = 7.60), 2.93(6H, s). $^{13}$C NMR (500 MHz, $CDCl_3$, $\delta$)(ppm): 167.39, 161.95, 151.26, 149.67, 148.58, 148.44, 148.12, 146.06, 143.86, 143.61, 143.30, 138.46, 138.36, 138.19, 131.90, 131.84, 131.93, 131.31, 127.69, 126.29, 124.94, 124.61, 123.75, 123.19, 123.08, 122.65, 119.91, 119.72, 117.93, 117.48, 115.90, 112.33, 40.36 Ir-TRH: TRH (20.73 mg, 0.0932 mmol) was refluxed 4 h at 80 °C with $[Ir(ppy)_2]_2Cl_2$ (50 mg, 0.0932 mmol) in dichloromethane and methanol (3:1) solution to afford a reddish-orange colored solution. The solvent was evaporated under reduced pressure. The reddish-orange solid so obtained was redissolved in the minimum amount of dichloromethane and purified by a thin layer chromatography technique using 5% methanol in $CH_2Cl_2$. The desired orange solution was collected and dried under reduced pressure. This compound has been previously reported by


https://doi.org/10.1021/acs.jmedchem.4c01997
J. Med. Chem. 2024, 67, 20559−20570

us.[32] Yield: 44 mg (62%). HPLC Purity: ≥ 96%. Reproduced with permission from ref (32). Copyright 2024, Wiley-VCH.

Mass: Observed: $[M]^+$ = 723.1896; $[M]^+$: Exact: 723.1844. Reproduced with permission from ref (32). Copyright 2024, Wiley-VCH. $^1$H NMR (500 MHz, $CDCl_3$, $\delta$)(ppm): 10.02(1H, d, $J$ = 4.45), 8.66(1H, d, $J$ = 6.25), 8.50(1H, s), 8.31(1H, d, $J$ = 5.05), 8.06(1H, d, $J$ = 5.80), 7.91(1H, d, $J$ = 8.20), 7.88(1H, d, $J$ = 6.25), 7.80(2H, d, $J$ = 5.65), 7.70−7.68(2H, m), 7.64(1H, s), 7.55(1H, d, $J$ = 9.00), 7.52(1H, d, $J$ = 6.70), 7.41(1H, d, $J$ = 7.95), 7.35(1H, d, $J$ = 5.00), 7.29(1H, d, $J$ = 7.45), 7.17(1H, d, $J$ = 7.30), 7.07(1H, d, $J$ = 7.45), 7.02(1H, d, $J$ = 8.10), 6.92(1H, t, $J$ = 8.85), 6.81(1H, d, $J$ = 7.35), 6.75(1H, d, $J$ = 7.35), 6.43(1H, d, $J$ = 7.80), 6.30−6.28(1H, m), 6.24(1H, d, $J$ = 8.40). Reproduced with permission from ref (32). Copyright 2024, Wiley-VCH. $^{13}$C NMR (400 MHz, $CDCl_3$, $\delta$)(ppm): 168.36, 167.28, 151.03, 149.49, 148.69, 148.38, 147.91, 147.50, 145.74, 143.75, 143.57, 143.27, 138.57, 138.46, 131.84, 131.74, 130.93, 130.31, 129.53, 129.05, 128.94, 128.61, 128.09, 126.61, 124.95, 124.62, 124.37, 123.75, 123.25, 123.13, 122.71, 119.94, 119.80, 117.56. Reproduced with permission from ref (32). Copyright 2024, Wiley-VCH.

Ir-TRF: TRF (24 mg, 0.0932 mmol) was refluxed 4 h at 80 °C with $[Ir(ppy)_2]_2Cl_2$ (50 mg, 0.0932 mmol) in dichloromethane and methanol (3:1) solution to afford a reddish-orange colored solution. The solvent was evaporated under reduced pressure. The reddish-orange solid so obtained was redissolved in the minimum amount of dichloromethane and purified by a thin layer chromatography technique using 5% methanol in $CH_2Cl_2$. The desired orange solution was collected and dried under reduced pressure. Yield: 47 mg (66%). HPLC Purity: ≥ 95%.

ESI-MS: Observed $M^+$ = 759.1531; Exact $M^+$ = 759.1656 $^1$H NMR (500 MHz, $CDCl_3$, $\delta$)(ppm): 11.94(1H, s), 9.99(1H, s), 8.33(1H, br), 7.96−7.92(2H, dd, $J$ = 8.30), 7.83−7.77(3H, m), 7.70−7.67(3H, m), 7.64(2H, d, $J$ = 5.70), 7.50(1H, d, $J$ = 5.45), 7.43(1H, t, $J$ = 6.25), 7.07−7.00(4H, m), 6.94−6.89(2H, m), 6.74(1H, d, $J$ = 6.85), 6.27(2H, d, $J$ = 7.55). $^{13}$C NMR (500 MHz, $CDCl_3$, $\delta$)(ppm): 168.52, 167.39, 149.50, 149.14, 148.83, 148.37, 147.99, 147.23, 145.37, 143.73, 143.50, 143.19, 138.66, 138.57, 131.78, 131.06, 130.49, 126.03, 125.03, 124.72, 123.81, 123.40, 123.16, 122.93, 120.04, 119.88, 117.72, 109.85, 109.67, 104.82. $^{19}$F NMR (proton-coupled) (500 MHz, $CDCl_3$, $\delta$)(ppm): −108.09(t, $J$ = 10.00). $^{19}$F NMR (proton decoupled) (500 MHz, $CDCl_3$, $\delta$)(ppm): −108.09.

**Purity Assessment of Ir-TRN, Ir-TRH, and Ir-TRF.** The purity of the complexes Ir-TRN and Ir-TRF was determined using HPLC under the same conditions, while Ir-TRH was analyzed separately. For both Ir-TRN and Ir-TRF, HPLC was conducted on a C-18 reverse-phase column with a flow rate of 0.5 mL/min and UV detection at 300 nm, employing a linear gradient of 2% Solvent B (Water) in Solvent A (Acetonitrile) over 30 min. In the case of Ir-TRH, the analysis was performed using an AD-H column (250 × 4.6 mm) at a flow rate of 1 mL/min, with UV detection at 300 nm and applying a linear gradient of 10% Solvent B (iPrOH) in Solvent A (*n*-Hexane) over 20 min. This analytical method confirmed that all compounds had a purity level of ≥95%.

**Cells and Cell Lines.** ME-180 cells were obtained from ATCC - HTB-33 and cultured in Roswell Park Memorial Institute (RPMI) medium, supplemented with 10% Fetal bovine serum (Invi-trogen) and 1% penicillin−streptomycin (Gibco).

**MTT Assay.** Cell viability was assessed using the MTT (3-(4, 5-dimethyl thiazolyl-2)-2, 5-diphenyltetrazolium bromide) assay.[33] Cell viability was assessed using the MTT assay. ME-180, A549 and HaCaT cells were seeded at 10,000 cells per well in 96-well plates (Nunc, Denmark) and incubated overnight. The cells were then treated for 24 h with various doses of three different drugs: Ir-TRN, Ir-TRH, and Ir-TRF. All experiments used a growth medium containing 0.1% DMSO as a vehicle control. After incubation of 24 h with these complexes, a complete culture medium with MTT (Sigma-Aldrich) at a concentration of 0.5 mg/mL was added to each well and incubated for 4 h in a $CO_2$ incubator at 37 °C. The MTT solution was then removed, and the resulting purple formazan precipitates were dissolved by adding 100 $\mu$L of DMSO to each well. Absorbance was measured at 570 nm using a Varioskan LUX microplate reader (Thermo Scientific, Finland). All complex concentrations were tested in quadruplicate, and the experiments were repeated three times. The cytotoxic effects of the complexes were expressed as the percentage of viable cells compared to the vehicle control. A dose−response curve was generated using the log(inhibitor) vs response—Variable slope (four parameters) method with GraphPad Prism 5.0 (GraphPad Software, San Diego, CA, USA). The drug concentrations inhibiting cell growth by 25% ($IC_{25}$) and 50% ($IC_{50}$) were determined and used for further studies.

**Cell Migration Assay.** ME-180 cells were seeded in triplicates in 12-well plates and allowed to grow until they formed a confluent monolayer. A scratch/wound was created using a p200 pipet tip, with a reference line drawn using a marker pen. The cells were gently washed with PBS and cultured in their respective media with reduced serum (1%) containing a nontoxic dose of the iridium(III) complexes, less than the $IC_{25}$ dose, for 24 h. Images of two scratch areas from each well, both above and below the reference line, were taken at 0, 12, and 24 h using an inverted Nikon Eclipse Ts2 microscope (10×) (Tokyo, Japan). The scratch areas were measured using ImageJ software. Wound closure was quantified by calculating the percentage change in the normalized measurement area divided by the initial open area, using the formula: Wound Closure % = $[(X(0) - X(t))/X(0)] \times 100$, where X(0) is the area at time zero, and X(t) is the area after the incubation time.[34]

**Protein Isolation and Western Blot.** ME-180 cells were treated with $IC_{25}$ dose of Ir-TRN, Ir-TRH, and Ir-TRF for 24 h. The cells were washed twice with ice-cold PBS and lysed in RIPA buffer containing a protease inhibitor cocktail for 30 min on ice. The supernatant was collected after centrifugation at 13,300 rpm for 15 min at 4 °C. Protein concentration was determined using the Pierce BCA protein assay kit (Thermo Scientific, Rockford, IL, USA). Equal amounts of protein from each sample were subjected to SDS-PAGE and transferred onto polyvinylidene difluoride (PVDF) membranes (Millipore, Bedford, MA). The membranes were blocked for 1 h at room temperature with 5% skimmed milk in TBST (Tris-buffered saline containing 0.1% v/v Tween-20) and then incubated overnight at 4 °C with primary antibodies against p53 (1:1000, BioBharati), ERK2/MAPK (1:1000, BioBharati), ERp29 (1:1000, Invitrogen) and Y-Actin (1:5000, BioBharati). After three washes in TBST (10 min each), the membranes were incubated with HRP-conjugated secondary antibodies for 1 h at room temperature, followed by three 10 min washes with TBST. The signal was detected using SuperSignal West Pico Chemiluminescent Substrate (Thermo Scientific) according to the manufacturer's instructions. Protein expression was quantified using ImageJ software, normalized to $\gamma$-Actin expression, and expressed as relative fold change compared to the vehicle control. Protein expression was quantified using ImageJ software, normalized to Y-Actin expression, and expressed as relative fold change compared to the vehicle control.[35]

**Cell Cycle Analysis.** For cell cycle analysis,[36] ME-180 cells were seeded into 6-well plates ($2.5 \times 10^5$ cells/well) in RPMI medium and overnight incubated at 37 °C for cell cycle analysis. The cells were then treated with the three complexes at their respective $IC_{25}$ dose and incubated for 24 h. Following the incubation, cells were trypsinized and washed with ice-cold PBS twice. Cells were then resuspended in 70% ethanol for fixation and incubated for 2 h. Next, cells were washed with ice-cold PBS twice and incubated in PBS containing 50 $\mu$g/mL propidium iodide (PI), 100 $\mu$g/mL RNase A solution (Thermo Scientific), and 0.05% Triton X-100 for 20 min at 37 °C in the dark, followed by flow cytometric analysis (BD FACSVerse; BD Biosciences). FlowJo software (version 10.7.1) was used to analyze the Cell cycle distribution (G1/G0, S, and G2/M).

**Apoptosis Assay.** Apoptotic cells were analyzed using a Propidium Iodide staining method.[37] Apoptotic cells were analyzed using a Propidium Iodide staining method. ME-180 cells were seeded in a 96-well plate in its respective culture medium and overnight incubated at 37 °C. Cervical cancer cell lines were treated with the respective $IC_{50}$ dose of the 3 complexes or vehicle (0.1% DMSO) and incubated at 37 °C for 24 h. Following the incubation, cells were


https://doi.org/10.1021/acs.jmedchem.4c01997
J. Med. Chem. 2024, 67, 20559−20570

washed twice with PBS. Then, the cells were stained with Propidium Iodide and incubated for 15 min. The images were captured through a Nikon 0.3/OD75 microscope. The experiments were repeated thrice.

**Clonogenic Assay.** A clonogenic assay was performed to assess the impact of iridium(III) drugs on the colony-forming ability of ME-180 cells. Viable cells, ranging from 500 to 800, were plated in 60 mm dishes (Nunc, Denmark) and allowed to attach for 24 h. Following this period, the cells were treated with the iridium(III) complexes at their respective $IC_{25}$ doses and incubated for 24 h in a humidified $CO_2$ incubator. After the treatment period, the medium was replaced with a fresh RPMI medium, and the cells were incubated for another 7 to 10 days to allow colony formation. The cells were then fixed with 4% paraformaldehyde for 30mis and stained with 0.4% crystal violet for 45 min. After washing, colonies were manually counted, and the graph was plotted using the count of vehicle control v/s treated samples.

**DCFDA Assay.** To measure ROS generation after treatment with the iridium(III) complexes, the ME-180 cells were treated with the complexes and incubated for 24 h. Following incubation, the cells were incubated with 2′, 7′-dichlorodihydrofluorescein diacetate (DCFDA dye) for 30 min and then subjected to Flow cytometry analysis (BD FACSVerse; BD Biosciences) to measure the ROS generation. FlowJo software (version 10.7.1) was used to analyze the data.

**Statistical Analysis.** All experiments were conducted a minimum of three times, and the results are expressed as mean ± SEM. Comparisons among groups were made using a one-way analysis of variance followed by Dunnett's multiple comparison tests. All statistical analyses were performed with GraphPad Prism 6 (La Jolla, CA). A P value of <0.05 was deemed statistically significant.

## ■ ASSOCIATED CONTENT

### Supporting Information

The Supporting Information is available free of charge at https://pubs.acs.org/doi/10.1021/acs.jmedchem.4c01997.

ESI-Mass Spectra of complexes; $^{1}H$ NMR spectra of complexes; $^{13}C$ NMR spectra of complexes; $^{1}H-^{19}F$ NMR spectra of Ir-TRF;$^{19}F$ NMR spectra of Ir-TRF; HPLC trace of complexes; Electronic transitions of complexes; Frontier molecular orbitals (FMOs) of complexes; Cell viability data via Trypan Blue assay of complexes (PDF)

Molecular Formula Strings complexes (CSV)

## ■ AUTHOR INFORMATION


### Corresponding Authors

**Parna Gupta** − *Department of Chemical Sciences, Indian Institute of Science Education and Research-Kolkata, Mohanpur, West Bengal 741246, India;* orcid.org/0000-0002-5840-2841; Email: parna@iiserkol.ac.in

**Jayasri Das Sarma** − *Department of Biological Sciences, Indian Institute of Science Education and Research-Kolkata, Mohanpur, West Bengal 741246, India;* orcid.org/0000-0002-3980-4060; Email: dassarmaj@iiserkol.ac.in

### Authors

**Anushka Mondal** − *Department of Biological Sciences, Indian Institute of Science Education and Research-Kolkata, Mohanpur, West Bengal 741246, India*

**Bishnu Das** − *Department of Chemical Sciences, Indian Institute of Science Education and Research-Kolkata, Mohanpur, West Bengal 741246, India;* orcid.org/0000-0001-7194-3151

**Souvik Karmakar** − *Department of Biological Sciences, Indian Institute of Science Education and Research-Kolkata, Mohanpur, West Bengal 741246, India*

**Soumili Pani** − *Department of Biological Sciences and Department of Chemical Sciences, Indian Institute of Science Education and Research-Kolkata, Mohanpur, West Bengal 741246, India*

**Shrabani Khan** − *Department of Chemical Sciences, Indian Institute of Science Education and Research-Kolkata, Mohanpur, West Bengal 741246, India*

Complete contact information is available at: https://pubs.acs.org/10.1021/acs.jmedchem.4c01997


### Author Contributions

[§]A. M. and B. D. authors contributed equally. The manuscript was written through contributions of all authors. All authors have given approval to the final version of the manuscript.

### Notes

The authors declare no competing financial interest.

## ■ ACKNOWLEDGMENTS

J.D.S. and P.G. acknowledge IISER Kolkata for financial support and access to instrumental facilities. J.D.S acknowledges System Medicine Cluster (SyMeC) by the DBT grant (BT/MED II/NIBMG/SYMEC/2014/Vol.II) for providing financial support and access to instrumental facilities. P.G. also acknowledges the CSIR Grant 01/3028/21/EMR-II for financial support. The facilities and resources provided by the Chemical Sciences and Biological Sciences departments at IISER Kolkata were crucial for the successful completion of this work.

## ■ ABBREVIATIONS

| | |
|---|---|
| CuAAC | copper-catalyzed azide−alkyne cycloaddition |
| ER | endoplasmic reticulum |
| MMPs | metalloproteinases |
| MLCT | metal to ligand charge transfer |
| ROS | reactive oxygen species |

## ■ REFERENCES


(1) Brisson, M.; Drolet, M. Global elimination of cervical cancer as a public health problem. *Lancet Oncol.* **2019**, *20* (3), 319−321.

(2) Biemar, F.; Foti, M. Global progress against cancer-challenges and opportunities. *Cancer Biol. Med.* **2013**, *10* (4), 183−186.

(3) Ferlay, J.; Colombet, M.; Soerjomataram, I.; Parkin, D. M.; Piñeros, M.; Znaor, A.; Bray, F. Cancer statistics for the year 2020: An overview. *Int. J. Cancer* **2021**, *149* (4), 778−789.

(4) Sharma, P.; Jhawat, V.; Mathur, P.; Dutt, R. Innovation in cancer therapeutics and regulatory perspectives. *Med. Oncol.* **2022**, *39*, 76.

(5) Zhang, C.; Xu, C.; Gao, X.; Yao, Q. Platinum-based drugs for cancer therapy and antitumor strategies. *Theranostics* **2022**, *12* (5), 2115−2132.

(6) Casini, A.; Pöthig, A. Metals in Cancer Research: Beyond Platinum Metallodrugs. *ACS Cent. Sci.* **2024**, *10* (2), 242−250.

(7) Adhikari, S.; Nath, P.; Das, A.; Datta, A.; Baildya, N.; Duttaroy, A. K.; Pathak, S. A review on metal complexes and its anti-cancer activities: Recent updates from in vivo studies. *Biomed. Pharmacother.* **2024**, *171*, 116211.

(8) Lucaciu, R. L.; Hangan, A. C.; Sevastre, B.; Oprean, L. S. Metallo-Drugs in Cancer Therapy: Past, Present and Future. *Molecules* **2022**, *27* (19), 6485.

(9) Das, B.; Gupta, P. Multimetallic transition metal complexes: Luminescent probes for biomolecule sensing, ion detection, imaging and therapeutic application. *Coord. Chem. Rev.* **2024**, *504*, 215656.

(10) Liu, Z.; Sadler, P. J. Organoiridium Complexes: Anticancer Agents and Catalysts. *Acc. Chem. Res.* **2014**, *47* (4), 1174−1185.
(11) Das, B.; Gupta, P. Di 2-picolyl)amine appended luminescent probes: Advances in bioimaging and therapeutics. *Coord. Chem. Rev.* **2025**, *522*, 216209.
(12) Bi, X.-D.; Yang, R.; Zhou, Y.-C.; Chen, D.; Li, G.-K.; Guo, Y.-X.; Wang, M.-F.; Liu, D.; Gao, F. Cyclometalated Iridium(III) Complexes as High-Sensitivity Two-Photon Excited Mitochondria Dyes and Near-Infrared Photodynamic Therapy Agents. *Inorg. Chem.* **2020**, *59* (20), 14920−14931.
(13) Jin, C.; Liu, J.; Chen, Y.; Guan, R.; Ouyang, C.; Zhu, Y.; Ji, L.; Chao, H. Cyclometalated Iridium(III) Complexes as AIE Phosphorescent Probes for Real-Time Monitoring of Mitophagy in Living Cells. *Sci. Rep.* **2016**, *6*, 22039.
(14) Connell, T. U.; White, J. M.; Smith, T. A.; Donnelly, P. S. Luminescent Iridium(III) Cyclometalated Complexes with 1,2,3-Triazole "Click" Ligands. *Inorg. Chem.* **2016**, *55* (6), 2776−2790.
(15) Liu, S.; Müller, P.; Takase, M. K.; Swager, T. M. Click" Synthesis of Heteroleptic Tris-Cyclometalated Iridium(III) Complexes: Cu(I) Triazolide Intermediates as Transmetalating Reagents. *Inorg. Chem.* **2011**, *50* (16), 7598−7609.
(16) Das, B.; Gupta, P. Luminescent terpyridine appended geminal bisazide and bistriazoles: multinuclear Pt(II) complexes and AIPE-based DNA detection with the naked eye. *Dalton Trans.* **2021**, *50*, 10225−10236.
(17) Hohloch, S.; Suntrup, L.; Sarkar, B. Arene−Ruthenium(II) and − Iridium(III) Complexes with "Click"-Based Pyridyl-triazoles, Bistriazoles, and Chelating Abnormal Carbenes: Applications in Catalytic Transfer Hydrogenation of Nitrobenzene. *Organometallics* **2013**, *32* (24), 7376−7385.
(18) McCarney, E. P.; Hawes, C. S.; Blasco, S.; Gunnlaugsson, T. Synthesis and structural studies of 1,4-di(2-pyridyl)-1,2,3-triazole dpt and its transition metal complexes; a versatile and subtly unsymmetric ligand. *Dalton Trans.* **2016**, *45*, 10209−10221.
(19) Zhang, L.; Chinnathambi, A.; Alharbi, S. A.; Veeraraghavan, V. P.; Mohan, S. K.; Zhang, G. Punicalagin promotes the apoptosis in human cervical cancer (ME-180) cells through mitochondrial pathway and by inhibiting the NF-kB signaling pathway. *Saudi J. Biol. Sci.* **2020**, *27* (4), 1100−1106.
(20) Levine, A. J.; Momand, J.; Finlay, C. A. The p53 tumour suppressor gene. *Nature* **1991**, *351* (6326), 453−456.
(21) Hyun, S.-Y.; Jang, Y.-J. p53 activates $G_1$ checkpoint following DNA damage by doxorubicin during transient mitotic arrest. *Oncotarget* **2015**, *6* (7), 4804−4815.
(22) Shaw, P.; Bovey, R.; Tardy, S.; Sahli, R.; Sordat, B.; Costa, J. Induction of apoptosis by wild-type p53 in a human colon tumor-derived cell line. *Proc. Natl. Acad. Sci. U.S.A.* **1992**, *89* (10), 4495−4499.
(23) Marchese, V.; Juarez, J.; Patel, P.; Hutter-Lobo, D. Density-dependent ERK MAPK expression regulates MMP-9 and influences growth. *Mol. Cell. Biochem.* **2019**, *456* (1−2), 115−122.
(24) Zhang, W.; Liu, H. T. MAPK signal pathways in the regulation of cell proliferation in mammalian cells. *Cell Res.* **2002**, *12* (1), 9−18.
(25) Auten, R. L.; Davis, J. M. Oxygen Toxicity and Reactive Oxygen Species: The Devil Is in the Details. *Pediatr. Res.* **2009**, *66*, 121−127.
(26) Rao, R. V.; Bredesen, D. E. Misfolded proteins, endoplasmic reticulum stress and neurodegeneration. *Curr. Opin. Cell Biol.* **2004**, *16* (6), 653−662.
(27) Ohsawa, Y.; Sprouse, S.; King, K. A.; DeArmond, M. K.; Hanck, K. W.; Watts, R. J. Electrochemistry and spectroscopy of ortho-metalated complexes of iridium(III) and rhodium(III). *J. Phys. Chem.* **1987**, *91* (5), 1047−1054.
(28) Frisch, M. J.; Trucks, G. W.; Schlegel, H. B.; Scuseria, G. E.; Robb, M. A.; Cheeseman, J. R.; Scalmani, G.; Barone, V.; Petersson, G. A.; Nakatsuji, H.; Li, X.; Caricato, M.; Marenich, A. V.; Bloino, J.; Janesko, B. G.; Gomperts, R.; Mennucci, B.; Hratchian, H. P.; Ortiz, J. V.; Izmaylov, A. F.; Sonnenberg, J. L.; Wil-liams-Young, D.; Ding, F.; Lipparini, F.; Egidi, F.; Goings, J.; Peng, B.; Petrone, A.; Henderson, T.; Ranasinghe, D.; Zakrzewski, V. G.; Gao, J.; Rega, N.; Zheng, G.; Liang, W.; Hada, M.; Ehara, M.; Toyota, K.; Fuku-da, R.; Hasegawa, J.; Ishida, M.; Nakajima, T.; Honda, Y.; Kitao, O.; Nakai, H.; Vreven, T.; Throssell, K.; Montgomery, J. A., Jr.; Peralta, J. E.; Ogliaro, F.; Bearpark, M. J.; Heyd, J. J.; Brothers, E. N.; Kudin, K. N.; Staroverov, V. N.; Keith, T. A.; Kobayashi, R.; Normand, J.; Raghavachari, K.; Rendell, A. P.; Burant, J. C.; Iyengar, S. S.; Tomasi, J.; Cossi, M.; Millam, J. M.; Klene, M.; Adamo, C.; Cammi, R.; Ochterski, J. W.; Martin, R. L.; Morokuma, K.; Farkas, O.; Foresman, J. B.; Fox, D. J. *Gaussian 16*. Revision C.01; Gaussian, Inc.: Wallingford CT, 2016.
(29) Amen, O. M.; Sarker, S. D.; Ghildyal, R.; Arya, A. Endoplasmic Reticulum Stress Activates Unfolded Protein Response Signaling and Mediates Inflammation, Obesity, and Cardiac Dysfunction: Therapeutic and Molecular Approach. *Front. Pharmacol.* **2019**, *10*, 977.
(30) Fribley, A.; Zhang, K.; Kaufman, R. J. Regulation of Apoptosis by the Unfolded Protein Response. *Methods Mol. Biol.* **2009**, *559*, 191−204.
(31) Abdullah, A.; Ravanan, P. Kaempferol mitigates Endoplasmic Reticulum Stress Induced Cell Death by targeting caspase 3/7. *Sci. Rep.* **2018**, *8* (1), 2189.
(32) Das, B.; Biswas, P.; Mallick, A. I.; Gupta, P. Application of Mono and Trinuclear Cyclometalated Iridium (III) Complexes in Differential Bacterial Imaging and Antimicrobial Photodynamic therapy. *Chem.—Eur. J.* **2024**, *30* (36), No. e202400646.
(33) Deng, Y.; Li, Y.; Yang, F.; Zeng, A.; Yang, S.; Luo, Y.; Zhang, Y.; Xie, Y.; Ye, T.; Xia, Y.; Yin, W. The extract from Punica granatum (pomegranate) peel induces apoptosis and impairs metastasis in prostate cancer cells. *Biomed. Pharmacother.* **2017**, *93*, 976−984.
(34) Kumar, S.; Mulchandani, V.; Sarma, J. D. Methanolic neem (Azadirachta indica) stem bark extract induces cell cycle arrest, apoptosis and inhibits the migration of cervical cancer cells in vitro. *BMC Complementary Med. Ther.* **2022**, *22* (1), 239.
(35) Treloar, K. K.; Simpson, M. J. Sensitivity of Edge Detection Methods for Quantifying Cell Migration Assays. *PLoS One* **2013**, *8* (6), No. e67389.
(36) Kim, K. H.; Sederstrom, J. M. Assaying Cell Cycle Status Using Flow Cytometry. *Curr. Protoc. Mol. Biol.* **2015**, *111*, 28.6.1−28.6.11.
(37) Das, B.; Gupta, S.; Mondal, A.; Kalita, K. J.; Mallick, A. I.; Gupta, P. Tuning the Organelle-Specific Imaging and Photodynamic Therapeutic Efficacy of Theranostic Mono- and Trinuclear Organometallic Iridium(III) Complexes. *J. Med. Chem.* **2023**, *66* (22), 15550−15563.


https://doi.org/10.1021/acs.jmedchem.4c01997
*J. Med. Chem.* 2024, 67, 20559−20570